


Theoretical calculations for the capture cross section of the formation of heavy and superheavy nuclei

Guang Jin Li (黎广金) and Xiao Jun Bao (包小军)^{*}

Department of Physics, Collaborative Innovation Center for Quantum Effects, and Key Laboratory of Low Dimensional Quantum Structures and Quantum Control of Ministry of Education, Hunan Normal University, Changsha 410081, People's Republic of China

 (Received 1 January 2023; accepted 6 February 2023; published 21 February 2023)

Capture cross section of formation heavy nuclei and superheavy nuclei with charge number $Z = 84\text{--}118$ are systematically studied based on an empirical coupled-channel model, in which different barrier distribution functions are constructed according to the different coupling modes between target and projectile. The calculated results are in good agreement with the experimental data for most of reaction systems. The reason for the difference between the theoretical results and the experimental values have been analyzed.

DOI: [10.1103/PhysRevC.107.024611](https://doi.org/10.1103/PhysRevC.107.024611)

I. INTRODUCTION

Nuclear fusion in heavy-ion collisions is a dynamical processes of quantum many-body systems [1–5]. Theoretically, the simplest approach for heavy-ion fusion reactions is to use the one-dimensional potential model where both the projectile and the target are assumed to be structureless [1,2]. The single-barrier penetration models have been applied to describe successfully the capture cross sections for light reaction systems around and above Coulomb barrier region [6]. Structural effects of target nuclei (ground state deformation) on the capture cross sections was first recognized [7,8], this seminal work has stimulated many experimental and theoretical works and subsequent experimental data clearly demonstrated this effect [7–9].

For the subbarrier fusion reactions, extensive experimental as well as theoretical studies have revealed that fusion reactions are strongly influenced by the couplings between the relative motion and nuclear intrinsic degrees of freedom on fusion reactions. Capture cross sections are enhanced by orders of magnitude as a result of coupling to collective modes of the interacting nuclei [10–20]. In recent works, the capture cross sections hindrance far below the barrier is discussed [21,22]. Various theoretical approaches have been developed to explore the fusion excitation function or capture process at the subbarrier energies.

The overall description and understanding of the heavy-ion fusion excitation function, covering the whole energy range from the extreme subbarrier region up to high above the Coulomb barrier [23], becomes an important topic in reaction theory and experiment studies [24]. One of reasons is that the overall uncertainties in predicting heavy and superheavy nuclei synthesis cross sections are associated with the calculations of capture cross sections [25–27]. The main reason is that fusion dynamics is closely related to nuclear

structure of the interacting nuclei caused a dramatic effect on heavy-ion capture cross sections [28–36]. This is because the nucleus-nucleus potential is modified by nuclear structure and dynamically by the interaction.

There are several models for capture cross sections. Each of them has been tested against a number of measurements of capture cross sections for reactions that, mostly, do not lead to the formation of the superheavy nuclei.

The formation cross section of compound nucleus is a basic process in the fusion reaction to synthesize new nuclides and new elements. To describe the whole fusion process much reasonably, the accurate calculation of the capture cross section is particularly important [37]. The main goal of the present paper is to examine capture process for the synthesis mechanism of heavy and superheavy nuclei carefully. We perform a systematic study of capture cross sections from heavy to superheavy nuclei by the different coupling modes between target and projectile.

II. THEORETICAL FRAMEWORK

The capture cross section at a given center-of-mass energy $E_{c.m.}$ can be written as the sum of the cross section for each partial wave J [7,38,39]:

$$\sigma_{\text{cap}}(E_{c.m.}) = \frac{\pi \hbar^2}{2\mu E_{c.m.}} \sum_J (2J+1) T(E_{c.m.}, J), \quad (1)$$

where σ_{cap} is the capture cross section, $E_{c.m.}$ and J separately represent the incident energy in the center-of-mass system and relative angular momentum. $T(E_{c.m.}, J)$ is the penetration probability of the two colliding nuclei overcoming the Coulomb potential barrier in the entrance channel.

For the single-barrier penetration model, the interaction potential around the Coulomb barrier B can be approximated by an inverted parabola, the analytical expression for the penetration probability is given by the well-known Hill-Wheeler

^{*}baoxiaojun@hunnu.edu.cn

formula [40,41]

$$T^{\text{HW}}(E_{\text{c.m.}}, J, B) = \frac{1}{1 + \exp \left\{ -\frac{2\pi}{\hbar\omega_B(J)} \left[E_{\text{c.m.}} - B - \frac{\hbar^2}{2\mu R_B^2(J)} J(J+1) \right] \right\}}, \quad (2)$$

where $\hbar\omega_B(J)$ is the width of the parabolic Coulomb barrier at the position $R_B(J)$, and B is the Coulomb barrier.

In the real case the nucleus-nucleus interaction potential is a multidimensional surface and the incoming flux overcomes the Coulomb barrier at different values of its height B . Therefore, the capture cross section $\sigma_{\text{cap}}(E_{\text{c.m.}})$ can be estimated by using the empirical coupled-channel method. The empirical channel coupling model has been proposed for a simple estimation of multidimensional barrier penetrability based on the idea of the barrier distribution function. Various types of distribution functions are used.

In the present work, according to the different coupling modes between target and projectile, we construct different barrier distribution functions. There are three cases: (i) fusion reactions involving two spherical nuclei, (ii) reactions with two statically deformed nuclei, and (iii) reactions with the combination of one spherical nucleus and one statically deformed nucleus.

Two spherical nuclei mainly depend on coupling of their relative motion to surface vibrations. Thus, the Coulomb barrier mainly depends on dynamical deformations. The total penetration probability in Eq. (1) should be averaged over barrier height B ,

$$T(E_{\text{c.m.}}, J) = \int f(B) T^{\text{HW}}[E_{\text{c.m.}}, J, B] dB, \quad (3)$$

where the normalized function $f(B)$ may be approximated by an asymmetric Gaussian form

$$f(B) = \begin{cases} \frac{1}{N} \exp \left[-\left(\frac{B-B_m}{\Delta_1} \right)^2 \right], & B < B_m \\ \frac{1}{N} \exp \left[-\left(\frac{B-B_m}{\Delta_2} \right)^2 \right], & B > B_m. \end{cases}$$

Here, N is the normalization constant. The $B_m = aB_0 + (1-a)B_S$ is central value of barrier distribution. The value of quantity B_S corresponds to minimal value of the two-dimensional barrier depended on dynamical deformations, and B_0 is defined as the Coulomb barrier of spherical nuclei. $\Delta_1 = bE_D$ and $\Delta_2 = cE_D$ are left and right width, respectively. E_D is the deformation energy of the reaction system at the saddle point. The parameters $a = 0.26$ ($Z_p Z_T < 1150$) and $a = 0.50$ ($Z_p Z_T \geq 1150$), $b = 0.32$ and $c = 0.93$ of the barrier distribution are taken from Ref. [38]. Details of parameters determination are shown in Ref. [38].

For statically deformed nuclei, the penetration probability should be averaged over the orientations of both nuclei. Therefore, the total penetration probability in Eq. (1) is given by

$$T(E_{\text{c.m.}}, J) = \frac{1}{4} \int_0^\pi \int_0^\pi T^{\text{HW}}[E_{\text{c.m.}}, J, B(\beta_1, \theta_1, \beta_2, \theta_2)] \times \sin \theta_1 \sin \theta_2 d\theta_1 d\theta_2,$$

where $B(\beta_1, \theta_1, \beta_2, \theta_2)$ is the orientation dependent barrier, and β_1 and β_2 are the static deformation parameters of interacting nuclei.

If one of the interacting projectile and target nuclei is a spherical nuclei in ground state and the other is a statically deformed nucleus, the interaction barrier distribution is mainly caused by the different orientation effects of the deformed nucleus and the spherical (or nearly spherical) nucleus are caused by dynamical deformation.

One may parametrize the barrier B for the arbitrary value of the projectile deformation (β_1) and target orientation (θ_2) as follows:

$$B(\theta_2, \beta_1) = B' + [B(\theta_2, 0) - B(0, 0)], \quad B' = B(0, \beta_1). \quad (4)$$

For spherical projectile and statically deformed target, the penetration probability should be averaged over the deformation-dependent barrier height as well as the orientations of both nuclei. Then the total penetration probability in Eq. (1) is given by

$$T(E_{\text{c.m.}}, J) = \frac{1}{2} \int \sin \theta_2 d\theta_2 \int f(B') T^{\text{HW}} \times [E_{\text{c.m.}}, J, B(\theta_2, \beta_1)] dB', \quad (5)$$

In the present work, the interaction potential is one of the key quantities in the calculation of the penetration probability. The effective interaction potential of the two nuclei consists of the long-range Coulomb repulsive potential, the attractive short-range nuclear potential, and the deformation potential energy

$$V(r, \beta_1, \beta_2, \theta_1, \theta_2) = V_C(r, \beta_1, \beta_2, \theta_1, \theta_2) + V_N(r, \beta_1, \beta_2, \theta_1, \theta_2) + \frac{1}{2} C_1 (\beta_1 - \beta_1^0)^2 + \frac{1}{2} C_2 (\beta_2 - \beta_2^0)^2. \quad (6)$$

The Coulomb potential can be calculated by Wong's formula [7] as the following:

$$V_C(r, \beta_1, \beta_2, \theta_1, \theta_2) = \frac{Z_1 Z_2 e^2}{r} + \left(\frac{9}{20\pi} \right)^{1/2} \left(\frac{Z_1 Z_2 e^2}{r^3} \right) \times \sum_{i=1}^2 R_i^2 \beta_i P_2(\cos \theta_i) + \left(\frac{3}{7\pi} \right) \left(\frac{Z_1 Z_2 e^2}{r^3} \right) \times \sum_{i=1}^2 R_i^2 [\beta_i P_2(\cos \theta_i)]^2, \quad (7)$$

where $P_2(\cos \theta_i)$ is the Legendre polynomial.

Many approaches have been developed to estimate the nuclear potential $V_N(R)$. In the present work, the double folding potential which belongs to the nuclear potential have been adopted. One standard method is to fold a nucleon-nucleon interaction with the projectile and target densities [42]. Thus

the nuclear potential reads

$$\begin{aligned}
 & V_N(R, \beta_1, \beta_2, \theta_1, \theta_2) \\
 &= C_0 \left\{ \frac{F_{\text{in}} - F_{\text{ex}}}{\rho^0} \left[\int \rho_1^2(r) \rho_2(r - R) dr \right. \right. \\
 &\quad \left. \left. + \int \rho_1(r) \rho_2^2(r - R) dr \right] + F_{\text{ex}} \int \rho_1(r) \rho_2(r - R) dr \right\}, \quad (8)
 \end{aligned}$$

with

$$F_{\text{in,ex}} = f_{\text{in,ex}} + f'_{\text{in,ex}} \frac{N_1 - Z_1}{A_1} \frac{N_2 - Z_2}{A_2}, \quad (9)$$

where N_1 , N_2 and Z_1 , Z_2 are the neutron and proton numbers of the two nuclei, respectively. 1 and 2 represent the interacting projectile nucleus and target nucleus, respectively. Currently some parameters used are as follows: $C_0 = 300 \text{ MeV fm}^3$, $f_{\text{in}} = 0.09$, $f_{\text{ex}} = -2.59$, $f'_{\text{in}} = 0.42$, $f'_{\text{ex}} = 0.54$, $\rho^0 = 0.165 \text{ fm}^{-3}$. The nuclear density distribution functions $\rho_1(r)$ and $\rho_2(r)$ are two-parameter Woods-Saxon types:

$$\rho_1(r) = \frac{\rho^0}{1 + \exp[(r - \mathfrak{R}_1(\alpha_1)]/a_{\rho_1})}, \quad (10)$$

$$\rho_2(r) = \frac{\rho^0}{1 + \exp[|(r - R) - \mathfrak{R}_2(\alpha_2)]/a_{\rho_2}}. \quad (11)$$

The parameters a_{ρ_1} and a_{ρ_2} are the diffuseness of the two nuclei, respectively. The general value range is around 0.50–0.58. In the present work, the parameters $a_{\rho_1} = 0.52$ and $a_{\rho_2} = 0.52$ are adopted. In principle, the diffuseness of the two nuclei depend on the charge and mass numbers of the nucleus [42]. At present, the deformation parameters β_2 and β_4 of projectile and target are taken from Ref. [43].

III. NUMERICAL RESULTS AND DISCUSSIONS

A. Heavy-nuclei region

In the present work, we develop a set of methods to construct different barrier distribution functions according to the difference coupling modes of the projectile-target nucleus. To prove the validity of our model, the capture cross sections for formation compound nucleus of 52 heavy nuclei are systematically calculated by using double-folding potential. Our calculations for all projectile-target combinations were performed with one set of parameters and with the same assumptions.

For eight fusion reactions involving two spherical nuclei, the capture cross section σ_{cap} as a function of the incident energy $E_{\text{c.m.}}$ are shown in Fig. 1. The black arrow shows the values of Bass barrier [54]. For around and above the Coulomb barrier region and subbarrier energies, we compare the calculated results for the capture cross sections based on the double folding potential with experimental data. One finds that almost all capture cross sections using the double-folding potential agree with the experimental data.

For deeper subbarrier energies, the experimental results show that the capture cross section decreases very rapidly. Carefully observation can find that in the reactions $^{36}\text{S} + ^{206}\text{Pb}$ and $^{36}\text{S} + ^{208}\text{Pb}$, the theoretical results overestimated the

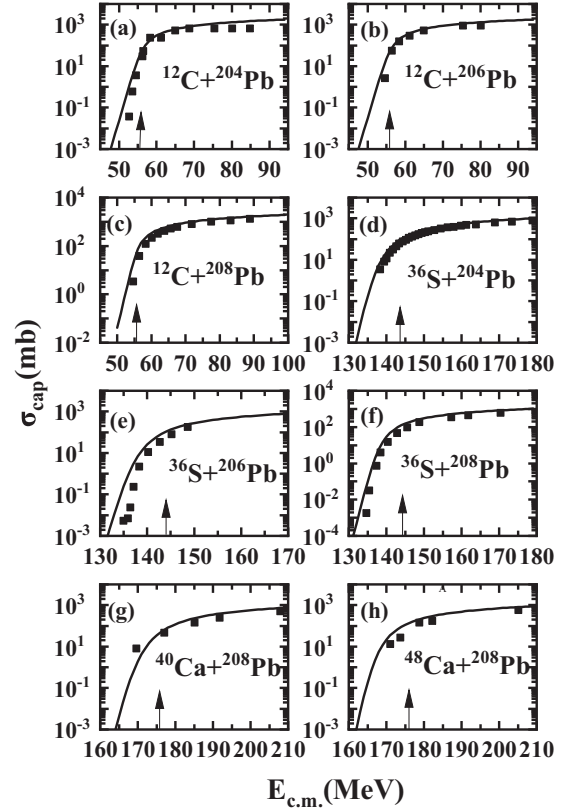


FIG. 1. The calculated and experimental capture cross sections for the reaction systems of $^{12}\text{C} + ^{204,206,208}\text{Pb}$, $^{36}\text{S} + ^{204,206,208}\text{Pb}$, and $^{40,48}\text{Ca} + ^{208}\text{Pb}$. The calculated results with the parameters $a_{\rho_1} = 0.52$, $a_{\rho_2} = 0.52$ are denoted by solid lines. The solid squares show the experimental values. The arrow indicates the Bass barrier. The experimental data were taken from Refs. [44–48].

experimental data. It is well know that for a span of incident energies of only a few MeV of the Bass barrier, in which the parabolic approximation remains valid. The exponential drop of capture cross section associated with the characteristic values of $\hbar\omega(J)$ in Eq. (2), which has limited in practice the range of calculated capture cross section using Eq. (2). From the systematic perspective of describing experimental data by theoretical model, our model cannot describe the experimental data of capture cross section at extreme subbarrier energies.

For 23 reactions with the combination of one spherical nucleus and one statically deformed nucleus, the calculated results are compared with the available experimental data in Figs. 2–5. It can be seen from Figs. 2–5 that the theoretical calculation results are reasonably reproduce the experimental data. However, careful comparison measured capture cross sections with the calculated results reveal that the calculated capture cross sections systematically deviated from the experimental data for $^{28}\text{Si} + ^{208}\text{Pb}$, $^{32}\text{S} + ^{208}\text{Pb}$, and $^{34}\text{S} + ^{204,206,208}\text{Pb}$ reaction systems at subbarrier energies in Figs. 3 and 4.

The deformation parameters used in present work are theoretical values calculated in the macroscopic-microscopic model [43], which can reproduce the experimental data [60]

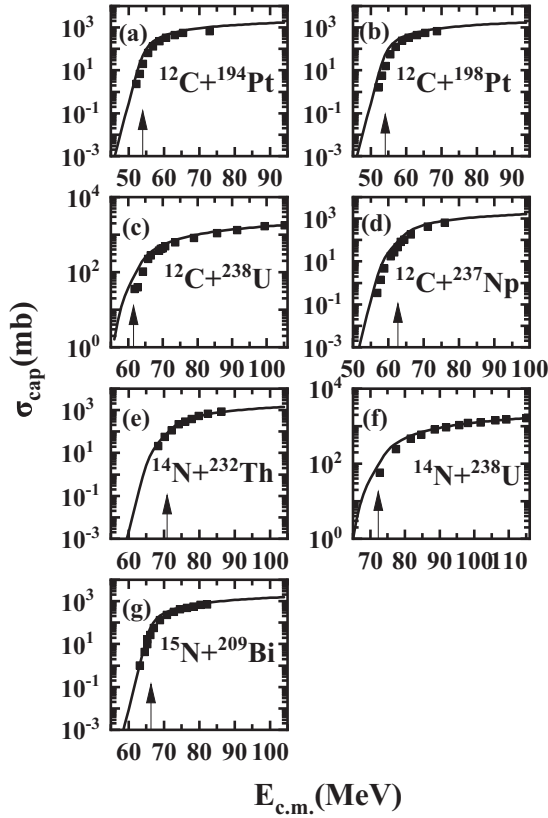


FIG. 2. The same as Fig. 1 but for $^{12}\text{C}+^{194,198}\text{Pt}$, $^{12}\text{C}+^{238}\text{U}$, $^{12}\text{C}+^{237}\text{Np}$, $^{14}\text{N}+^{232}\text{Th}$, $^{14}\text{N}+^{238}\text{U}$, and $^{15}\text{N}+^{209}\text{Bi}$ reactions. The experimental data were taken from Refs. [47,49–53].

well for deformation parameters in the heavy-nuclei region. However, in the light-nuclei region, there are significant differences between the theoretical calculation results and the experimental deformation parameters [60]. Heavy-ion fusion dynamics is intimately linked to nuclear deformation. Therefore, the nuclear deformation must be reliable to some extent.

To study the influence of deformation parameter on the capture cross section, the calculated capture cross section by using experimental quadrupole deformation of projectile nuclei for $^{28}\text{Si}+^{208}\text{Pb}$, $^{32}\text{S}+^{208}\text{Pb}$, and $^{34}\text{S}+^{204,206,208}\text{Pb}$ reaction systems are shown in Fig. 6. The results (dashed lines) obtained from theoretical quadrupole deformation of projectile nuclei are given in Fig. 6 for comparison. One find that the calculated capture cross sections using experimental quadrupole deformation of projectile nuclei agree with the experimental data for $^{28}\text{Si}+^{208}\text{Pb}$ and $^{32}\text{S}+^{208}\text{Pb}$ reaction systems. For $^{34}\text{S}+^{204,206,208}\text{Pb}$ reaction systems, the reason for the difference that still exist between the theoretical results and the experimental values will be further analyzed in the following discussion.

For projectile it is magic number nuclei in Fig. 5, the calculated capture cross sections systematically deviated from the experimental data for $^{40}\text{Ca}+^{192}\text{Os}$, $^{40}\text{Ca}+^{194}\text{Pt}$, and $^{40,48}\text{Ca}+^{197}\text{Au}$ reaction systems. One can see that at energies near and below the Coulomb barrier the theoretical calculation results underestimated the experimental data. Some uncertainty still remains in the our calculations of capture cross

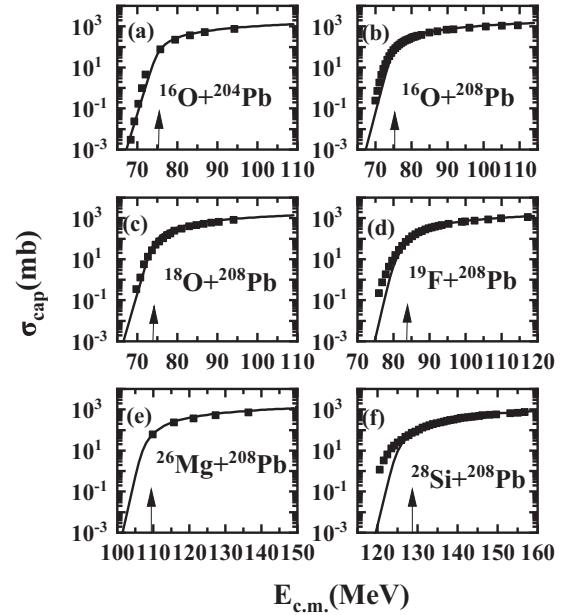


FIG. 3. The same as Fig. 1 but for $^{16}\text{O}+^{204,208}\text{Pb}$, $^{18}\text{O}+^{208}\text{Pb}$, $^{19}\text{F}+^{208}\text{Pb}$, $^{26}\text{Mg}+^{208}\text{Pb}$, and $^{28}\text{Si}+^{208}\text{Pb}$ reactions. The experimental data were taken from Refs. [53,55–59].

sections. For ^{40}Ca induced capture process, the large deviation may mainly arise from the unsuitable treatment of vibrational coupling of ^{40}Ca .

For 21 reactions with two statically deformed nuclei, the calculated results are compared with the available experimental data in Figs. 7–10. At first glance, one can see from each panel of Figs. 7–10 that the agreement of the calculated results with the experimental data is reasonably good. However, careful comparison measured capture cross sections with the calculated results reveal that the calculated capture cross sections systematically deviated from the experimental data for $^{20}\text{Ne}+^{238}\text{U}$, $^{27,29,31}\text{Al}+^{197}\text{Au}$, $^{28}\text{Si}+^{198}\text{Pt}$, $^{32}\text{S}+^{182,184}\text{W}$, and $^{39}\text{K}+^{181}\text{Ta}$ reaction systems at subbarrier energies.

The nuclear density distribution is very complicated, it is intimately linked to nuclear structure information. For the

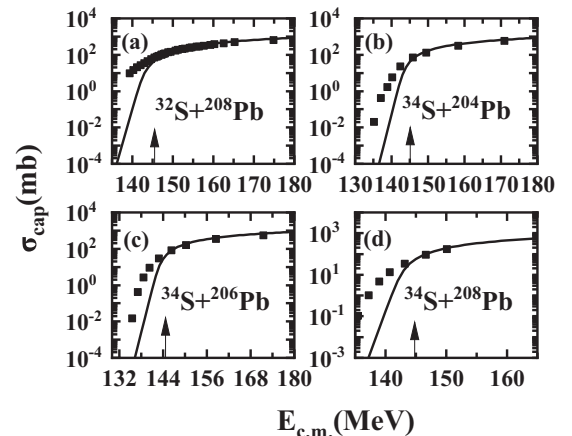


FIG. 4. The same comparison as presented in Fig. 1, but for $^{32}\text{S}+^{208}\text{Pb}$ [46] and $^{34}\text{S}+^{204,206,208}\text{Pb}$ [38] reactions.

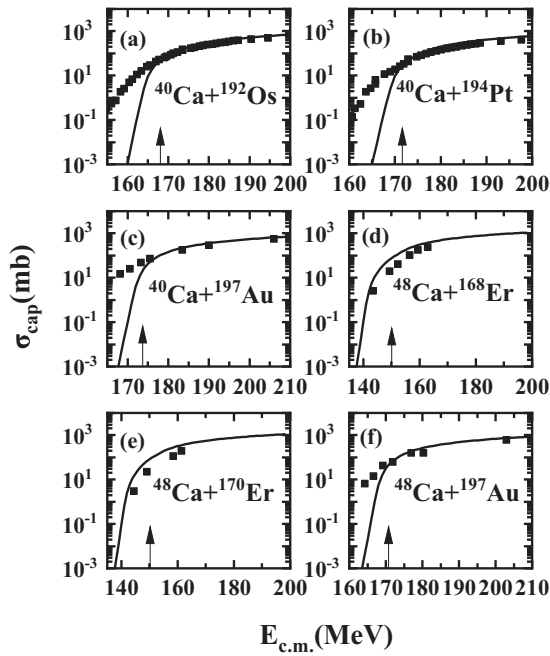


FIG. 5. The same comparison as presented in Fig. 1, but for $^{40}\text{Ca} + ^{192}\text{Os}$ [61], $^{40}\text{Ca} + ^{194}\text{Pt}$ [61], $^{40,48}\text{Ca} + ^{197}\text{Au}$ [48], and $^{48}\text{Ca} + ^{168,170}\text{Er}$ [44] reactions.

sake of simplicity, the surface diffuseness parameters of fixed values are adopted in our calculations. For all the above results, our calculations for all capture cross sections were performed with one set of parameters. The parameter

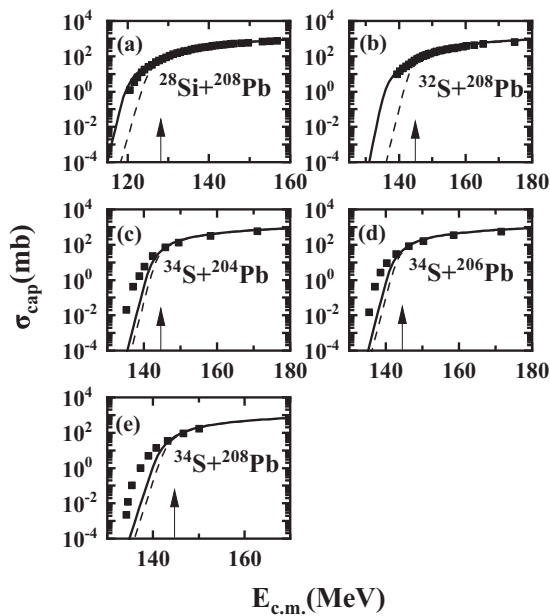


FIG. 6. The same comparison as presented in Fig. 1, but for $^{28}\text{Si} + ^{208}\text{Pb}$, $^{32}\text{S} + ^{208}\text{Pb}$, and $^{34}\text{S} + ^{204,206,208}\text{Pb}$ reactions. The solid and dashed lines denote the result based on the experimental values of quadrupole deformation and the theoretical value of the quadrupole deformation, respectively.

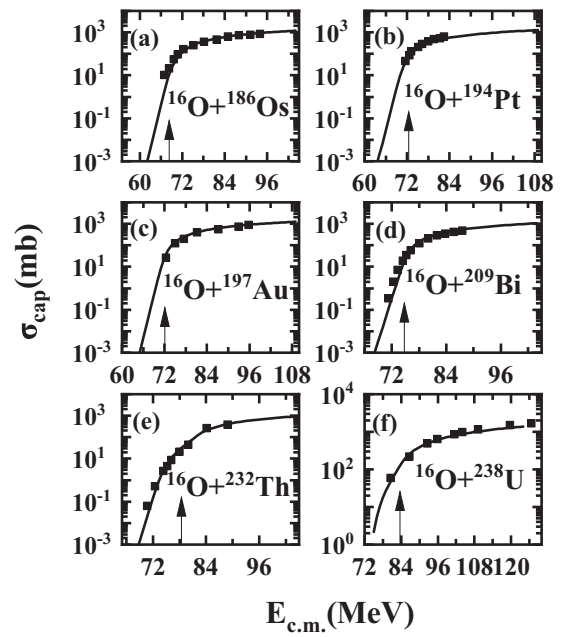


FIG. 7. The same comparison as presented in Fig. 1, but for $^{16}\text{O} + ^{186}\text{Os}$, $^{16}\text{O} + ^{194}\text{Pt}$, $^{16}\text{O} + ^{197}\text{Au}$, $^{16}\text{O} + ^{209}\text{Bi}$, $^{16}\text{O} + ^{232}\text{Th}$, and $^{16}\text{O} + ^{238}\text{U}$ reactions. The experimental data are taken from Refs. [50,53,62,63].

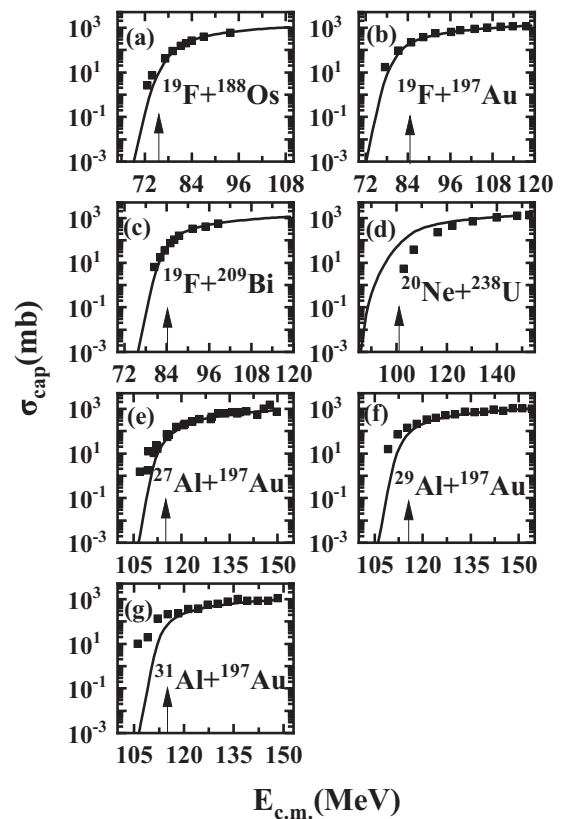


FIG. 8. The same comparison as presented in Fig. 1, but for $^{19}\text{F} + ^{188}\text{Os}$, $^{19}\text{F} + ^{197}\text{Au}$, $^{19}\text{F} + ^{209}\text{Bi}$, $^{20}\text{Ne} + ^{238}\text{U}$, $^{27}\text{Al} + ^{197}\text{Au}$, $^{29}\text{Al} + ^{197}\text{Au}$, and $^{31}\text{Al} + ^{197}\text{Au}$ reactions. The experimental data are taken from Refs. [63–65].

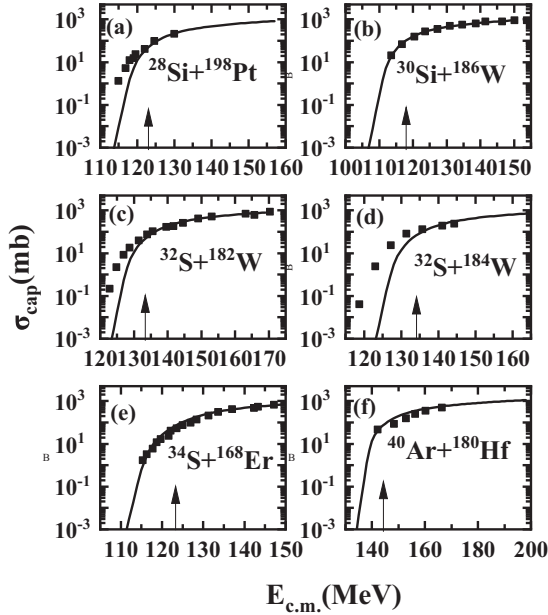


FIG. 9. The same comparison as presented in Fig. 1, but for $^{28}\text{Si}+^{198}\text{Pt}$, $^{30}\text{Si}+^{186}\text{W}$, $^{32}\text{S}+^{182,184}\text{W}$, $^{34}\text{S}+^{168}\text{Er}$, and $^{40}\text{Ar}+^{180}\text{Hf}$ reactions. The experimental data are taken from Refs. [63,66–69].

$a_{\rho 1} = 0.52$ and $a_{\rho 2} = 0.52$ represent the surface diffuseness of the nuclear density distribution. In fact, the $a_{\rho 1}$ and $a_{\rho 2}$ values are sensitive depends on the numbers of protons and neutrons in the nucleus. Therefore, we need to investigate the influence of the surface diffuseness parameter on capture the cross section.

The influence of the different values of the surface diffuseness parameters on the capture cross sections are shown in Fig. 11. Theoretical results obtained by the surface diffuseness parameter $a_{\rho 1} = 0.56$ and using experimental quadrupole deformation of projectile nuclei are shown by solid lines and those by the $a_{\rho 1} = 0.52$ and theoretical quadrupole deformation for projectile nuclei by dashed lines, respectively. Comparison of the calculated capture cross sections based on different surface diffuseness $a_{\rho 1} = 0.56$ (solid lines) and $a_{\rho 1} = 0.52$ (dashed lines) with the experimental data for the $^{32}\text{S}+^{182,184}\text{W}$, $^{32}\text{S}+^{208}\text{Pb}$, and $^{34}\text{S}+^{204,206,208}\text{Pb}$ reaction systems. The calculated results are in good agreement with the experimental data.

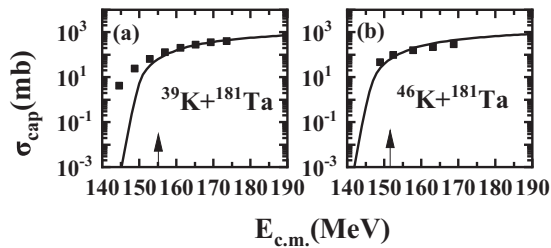


FIG. 10. The same comparison as presented in Fig. 1, but for $^{39}\text{K}+^{181}\text{Ta}$ and $^{46}\text{K}+^{181}\text{Ta}$ reactions. The experimental data are taken from Ref. [70].

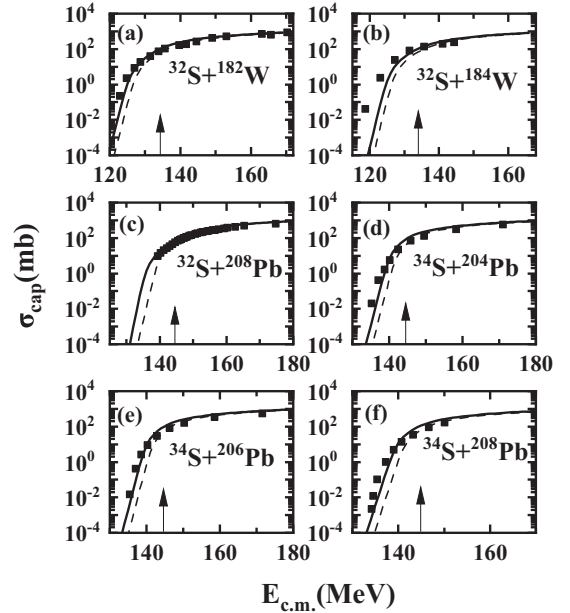


FIG. 11. The same comparison as presented in Fig. 1, but for $^{32}\text{S}+^{182,184}\text{W}$, $^{32}\text{S}+^{208}\text{Pb}$, and $^{34}\text{S}+^{204,206,208}\text{Pb}$ reactions. The solid and dashed lines denote the result based on the experimental values of quadrupole deformation and the theoretical value of the quadrupole deformation, respectively. The calculated results with the parameters $a_{\rho 1} = 0.56$, $a_{\rho 2} = 0.52$ are denoted by solid lines. The calculated results with the parameters $a_{\rho 1} = 0.52$, $a_{\rho 2} = 0.52$ are denoted by dashed lines.

B. Superheavy-nuclei region

For the synthesis of superheavy nuclei, the capture cross section σ_{cap} equals the sum of the quasifission, fast fission, fusion-fission, and fusion-evaporation residue cross sections. The coupling of channels plays an even more significant role in the fusion evaporation reaction. However, available experimental data on capture cross sections in the superheavy nuclear region are especially scarce. Therefore, theoretical calculations and predictions are of enormous importance in this region.

To test the effectiveness of our model for formation compound nucleus in superheavy nuclear region, the calculated results are compared with the available experimental data for synthesizing superheavy nuclei for 16 reaction systems in Figs. 12–14. Taking into account the experimental uncertainties one can say that the agreement between our calculated capture cross sections using double folding potential and the experimental values are good for many reaction systems except $^{52}\text{Cr}+^{208}\text{Pb}$, $^{48}\text{Ca}+^{246}\text{Cm}$, and $^{50}\text{Ti}+^{244}\text{Pu}$. The results of systematic calculation show that our theoretical model can describe the capture cross sections for formation compound nucleus in superheavy nuclear region. Since the calculations for all reactions were performed with the same parameters and assumptions, the accuracy of the description of the change trends of capture cross section with increasing charge number of formation compound nucleus is a certain degree of reliability.

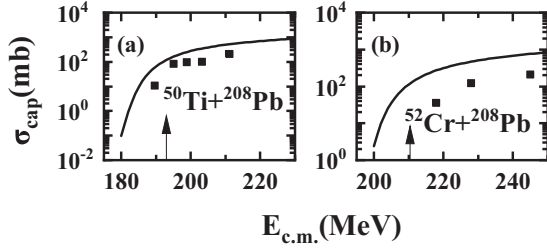


FIG. 12. The same comparison as presented in Fig. 1, but for $^{50}\text{Ti} + ^{208}\text{Pb}$ and $^{52}\text{Cr} + ^{208}\text{Pb}$ reactions. The experimental data are taken from Ref. [71].

It is well known that extensive experimental as well as theoretical studies have revealed that fusion reactions are strongly influenced by couplings of the relative motion of the colliding nuclei to several nuclear intrinsic motions. For heavier reaction systems at subbarrier energies, the calculated capture cross sections systematically deviated from the experimental data. For heavier systems, the dynamical kinetic-energy dissipation, which is another different mechanism from coupling, may begin to emerge and then suppress the capture probability seriously that calculated using Eq. (2).

The “bare” nucleus-nucleus interaction potential is extremely important ingredient in the low energy nuclear reaction calculations. In the present work, nuclear potential is obtained by the double-folding of the nuclear density with the density-dependent nucleon-nucleon interaction, the basic density distribution is still assumed as a simple sum of the densities of the target and projectile nuclei. Note that this approximation is valid only for the small overlap of the target and the projectile nuclei where they retain their

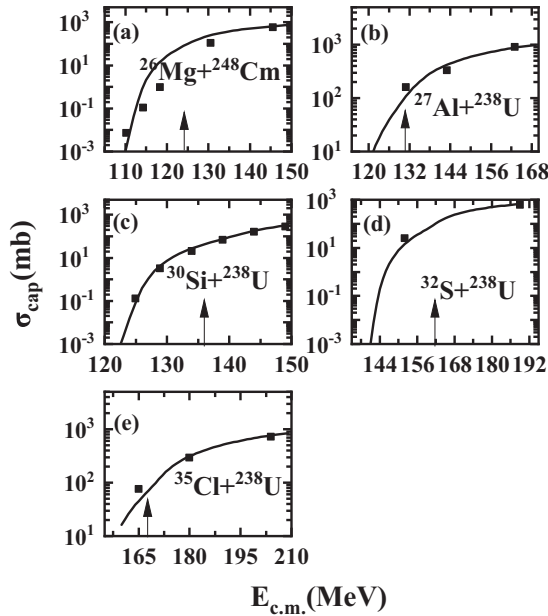


FIG. 13. The same comparison as presented in Fig. 1, but for $^{26}\text{Mg} + ^{248}\text{Cm}$, $^{27}\text{Al} + ^{238}\text{U}$, $^{30}\text{Si} + ^{238}\text{U}$, $^{32}\text{S} + ^{238}\text{U}$, and $^{35}\text{Cl} + ^{238}\text{U}$ reactions. The experimental data are taken from Refs. [72–74].

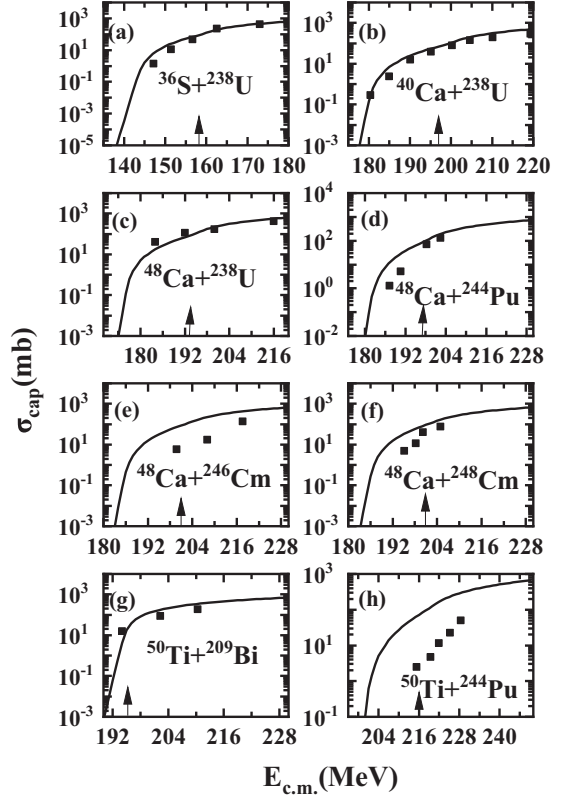


FIG. 14. The same comparison as presented in Fig. 1, but for $^{36}\text{S} + ^{238}\text{U}$, $^{40,48}\text{Ca} + ^{238}\text{U}$, $^{48}\text{Ca} + ^{244}\text{Pu}$, $^{48}\text{Ca} + ^{246,248}\text{Cm}$, $^{50}\text{Ti} + ^{209}\text{Bi}$, and $^{50}\text{Ti} + ^{244}\text{Pu}$ reactions. The experimental data are taken from Refs. [73,75–78].

individuality. In the present work, simple theoretical prescriptions were developed which directly introduced a distribution of barrier heights, the effect that results from the coupling to other (different orientations of the deformed nuclei and collective surface vibrations of the spherical nuclei) rather than relative distance degrees of freedom. The distribution of barriers around the single barrier leads to enhancement of the capture cross sections, at energies below that of the single barrier, because passage over the lower barriers is much more probable than penetration through the single barrier. Of course, the enhancement of the capture cross sections was a general phenomenon and not necessarily associated with the different orientations of the deformed nuclei and collective surface vibrations of the spherical nuclei. Therefore, the coupling between the relative motion and any nuclear degrees of freedom are important. In addition, the radial dependence of the nucleus-nucleus interaction potential at extremely close distances is extremely important problem. Some important work has been done on related issues [79–82]. Therefore the dynamical nucleus-nucleus potential and at extremely close distances has to be further studied by considering the distance between nuclear centers which is responsible for the capture cross section.

IV. SUMMARY

In summary, we construct different barrier distribution functions according to the different coupling modes between

target and projectile, the capture cross section of formation heavy nuclei and superheavy nuclei with charge number $Z = 84\text{--}118$ was systematically studied. The calculated results are in good agreement with the experimental results for most of reaction systems.

For some reaction systems at subbarrier energies, the calculated capture cross sections systematically deviated from the experimental data. Some uncertainty still remains in the our calculations of capture cross sections. For ^{40}Ca induced capture process, the large deviation may mainly arise from the unsuitable treatment the effects of collective surface vibrations on capture cross section. In addition, significant differences between the theoretical calculation deformation

parameters and the experimental deformation parameters in the light region, this leads to uncertainty in the present theoretical calculations. For heavier systems, the dynamical kinetic-energy dissipation, which is another different mechanism from coupling, may begin to emerge and then suppress the capture probability seriously that calculated using Eq. (2).

ACKNOWLEDGMENTS

The National Natural Science Foundation of China (Grants No. 12175064 and No. U2167203), Hunan Outstanding Youth Science Foundation (2022JJ10031) and Hunan Provincial Education Department (Key Project No. 20A290).

-
- [1] M. M. Beckerman, *Phys. Rep.* **129**, 145 (1985).
 [2] M. Dasgupta, D. J. Hinde, N. Rowley, and A. M. Stefanini, *Annu. Rev. Nucl. Part. Sci.* **48**, 401 (1998).
 [3] K. Hagino and N. Takigawa, *Prog. Theor. Phys.* **128**, 1061 (2012).
 [4] B. B. Back, H. Esbensen, C. L. Jiang, and K. E. Rehm, *Rev. Mod. Phys.* **86**, 317 (2014).
 [5] G. Montagnoli and A. M. Stefanini, *Eur. Phys. J. A* **53**, 169 (2017).
 [6] J. R. Birkelund, L. E. Tubbs, J. R. Huizenga, J. N. De, and D. Sperber, *Phys. Rep.* **56**, 107 (1979).
 [7] C. Y. Wong, *Phys. Rev. Lett.* **31**, 766 (1973).
 [8] R. G. Stokstad, Z. E. Switkowski, R. A. Dayras, and R. M. Wieland, *Phys. Rev. Lett.* **37**, 888 (1976).
 [9] N. Rowley, G. R. Satchler, and P. H. Stelson, *Phys. Lett. B* **254**, 25 (1991).
 [10] S. G. Steadman and M. J. Rhoades-Brown, *Annu. Rev. Nucl. Part. Sci.* **36**, 649 (1986).
 [11] K. Hagino, N. Rowley, and A. T. Kruppa, *Comput. Phys. Commun.* **123**, 143 (1999).
 [12] H. Esbensen, *Nucl. Phys. A* **352**, 147 (1981).
 [13] C. H. Dasso, S. Landowne, and A. Winther, *Nucl. Phys. A* **407**, 221 (1983).
 [14] C. H. Dasso, and G. Pollarolo, *Phys. Lett. B* **155**, 223 (1985).
 [15] C. H. Dasso and A. Vitturi, *Phys. Rev. C* **34**, 743 (1986).
 [16] K. Siwek-Wilczynska, E. Siemaszko, and J. Wilczynski, *Acta Phys. Pol. B* **33**, 451 (2002).
 [17] K. Siwek-Wilczynska and J. Wilczynski, *Phys. Rev. C* **69**, 024611 (2004).
 [18] H. Q. Zhang, C. J. Lin, F. Yang, H. M. Jia, X. X. Xu, Z. D. Wu, F. Jia, S. T. Zhang, Z. H. Liu, A. Richard, and C. Beck, *Phys. Rev. C* **82**, 054609 (2010).
 [19] H. M. Jia, C. J. Lin, L. Yang, X. X. Xu, N. R. Ma, L. J. Sun, F. Yang, Z. D. Wu, H. Q. Zhang, Z. H. Liu, and D. X. Wang, *Phys. Lett. B* **755**, 43 (2016).
 [20] A. V. Karpov, V. A. Rachkov, and V. V. Samarin, *Phys. Rev. C* **92**, 064603 (2015).
 [21] C. L. Jiang *et al.*, *Phys. Rev. Lett.* **89**, 052701 (2002).
 [22] C. L. Jiang *et al.*, *Phys. Rev. Lett.* **91**, 229202 (2003).
 [23] N. Wang, X. Z. Wu, Z. X. Li, M. Liu, and W. Scheid, *Phys. Rev. C* **74**, 044604 (2006).
 [24] C. L. Jiang, K. E. Rehm, B. B. Back, A. M. Stefanini, and G. Montagnoli, *Eur. Phys. J. A* **54**, 218 (2018).
 [25] W. Loveland, *Eur. Phys. J. A* **51**, 120 (2015).
 [26] X. J. Bao, S. Q. Guo, H. F. Zhang, and J. Q. Li, *J. Phys. G* **43**, 125105 (2016).
 [27] X. J. Bao, S. Q. Guo, H. F. Zhang, and J. Q. Li, *J. Phys. G* **44**, 045105 (2017).
 [28] G. P. A. Nobre and L. C. Chamon, L. R. Gasques, B. V. Carlson, and I. J. Thompson, *Phys. Rev. C* **75**, 044606 (2007).
 [29] A. Diaz-Torres, D. J. Hinde, and M. Dasgupta, G. J. Milburn, and J. A. Tostevin, *Phys. Rev. C* **78**, 064604 (2008).
 [30] V. V. Sargsyan, Z. Kanokov, G. G. Adamian, N. V. Antonenko, and W. Scheid, *Phys. Rev. C* **80**, 034606 (2009).
 [31] V. V. Sargsyan, G. G. Adamian, N. V. Antonenko, W. Scheid, and H. Q. Zhang, *Phys. Rev. C* **84**, 064614 (2011).
 [32] H. Esbensen and A. M. Stefanini, *Phys. Rev. C* **89**, 044616 (2014).
 [33] C. L. Jiang, K. E. Rehm, B. B. Back, H. Esbensen, R. V. F. Janssens, A. M. Stefanini, and G. Montagnoli, *Phys. Rev. C* **89**, 051603(R) (2014).
 [34] H. M. Jia, C. J. Lin, F. Yang, X. X. Xu, H. Q. Zhang, Z. H. Liu, Z. D. Wu, L. Yang, N. R. Ma, P. F. Bao, and L. J. Sun, *Phys. Rev. C* **89**, 064605 (2014).
 [35] V. A. Rachkov, A. V. Karpov, A. S. Denikin, and V. I. Zagrebaev, *Phys. Rev. C* **90**, 014614 (2014).
 [36] H. Esbensen, G. Montagnoli, and A. M. Stefanini, *Phys. Rev. C* **93**, 034609 (2016).
 [37] R. Kirchner, O. Klepper, W. Kurcewicz, E. Roeckl, E. Zganjar, E. Runte, W.-D. Schmidt-Ott, P. Tidemand-Petersson, N. Kaffrell, P. Peuser, and K. Rykaczewski, *Nucl. Phys. A* **378**, 549 (1982).
 [38] B. Wang, K. Wen, W. J. Zhao, E. G. Zhaob, and S. G. Zhou, *At. Data Nucl. Data Tables* **114**, 281 (2017).
 [39] V. I. Zagrebaev, Y. Aritomo, M. G. Itkis, Y. T. Oganessian, and M. Ohta, *Phys. Rev. C* **65**, 014607 (2001).
 [40] D. L. Hill and J. A. Wheeler, *Phys. Rev.* **89**, 1102 (1953).
 [41] V. I. Zagrebaev, *Phys. Rev. C* **64**, 034606 (2001).
 [42] G. G. Adamian, N. V. Antonenko, R. V. Jolos, S. P. Ivanova, and O. I. Melnikova, *Int. J. Mod. Phys. E* **05**, 191 (1996).
 [43] P. Möller, A. J. Sierk, T. Ichikawa, H. Sagawa, *At. Data Nucl. Data Tables* **109**, 1 (2016).
 [44] R. N. Sagaidak, G. N. Kniajeva, I. M. Itkis, M. G. Itkis, N. A. Kondratiev, E. M. Kozulin, I. V. Pokrovsky, A. I. Svirikhin, V. M. Voskressensky, A. V. Yeremin, L. Corradi, A. Gadea, A. Latina, A. M. Stefanini, S. Szilner, M. Trotta, A. M. Vinodkumar, S. Beghini, G. Montagnoli, F. Scarlassara *et al.*, *Phys. Rev. C* **68**, 014603 (2003).

- [45] A. Mukherjee, D. J. Hinde, M. Dasgupta, K. Hagino, J. O. Newton, and R. D. Butt, *Phys. Rev. C* **75**, 044608 (2007).
- [46] D. J. Hinde, M. Dasgupta, N. Herrald, R. G. Neilson, J. O. Newton, and M. A. Lane, *Phys. Rev. C* **75**, 054603 (2007).
- [47] J. Khuyagbaatar, K. Nishio, S. Hofmann, D. Ackermann, M. Block, S. Heinz, F. P. Heßberger, K. Hirose, H. Ikezoe, B. Kindler, B. Lommel, H. Makii, S. Mitsuoka, I. Nishinaka, T. Ohtsuki, Y. Wakabayashi, and S. Yan, *Phys. Rev. C* **86**, 064602 (2012).
- [48] A. J. Pacheco, J. O. Fernández Niello, D. E. DiGregorio, M. di Tada, J. E. Testoni, Y. Chan, E. Chávez, S. Gazes, E. Plagnol, and R. G. Stokstad, *Phys. Rev. C* **45**, 2861 (1992).
- [49] A. Shrivastava, S. Kailas, A. Chatterjee, A. Navin, A. M. Samant, P. Singh, S. Santra, K. Mahata, B. S. Tomar, and G. Pollarolo, *Phys. Rev. C* **63**, 054602 (2001).
- [50] V. E. Viola and T. Sikkeland, *Phys. Rev.* **128**, 767 (1962).
- [51] Z. Liu, H. Zhang, J. Xu, Y. Qiao, X. Qian, and C. Lin, *Phys. Rev. C* **54**, 761 (1996).
- [52] B. R. Behera, M. Satpathy, S. Jena *et al.*, *Phys. Rev. C* **69**, 064603 (2004).
- [53] E. Vulgaris, L. Grodzins, S. G. Steadman, and R. Ledoux, *Phys. Rev. C* **33**, 2017 (1986).
- [54] R. Bass, *Phys. Rev. Lett.* **39**, 265 (1977).
- [55] M. Dasgupta, D. J. Hinde, A. Diaz-Torres, B. Bouriquet, Catherine I. Low, G. J. Milburn, and J. O. Newton, *Phys. Rev. Lett.* **99**, 192701 (2007).
- [56] C. R. Morton, A. C. Berriman, M. Dasgupta, D. J. Hinde, J. O. Newton, K. Hagino, and I. J. Thompson, *Phys. Rev. C* **60**, 044608 (1999).
- [57] D. J. Hinde, A. C. Berriman, M. Dasgupta, J. R. Leigh, J. C. Mein, C. R. Morton, and J. O. Newton, *Phys. Rev. C* **60**, 054602 (1999).
- [58] D. J. Hinde, C. R. Morton, M. Dasgupta, J. R. Leigh, J. C. Mein, and H. Timmers, *Nucl. Phys. A* **592**, 271 (1995).
- [59] H. Sann, R. Bock, Y. T. Chu, A. Gobbi, A. Olmi, U. Lynen, W. Müller, S. Bjornholm, H. Esbensen, *Phys. Rev. Lett.* **47**, 1248 (1981).
- [60] S. Raman, C. W. Nestor, Jr., and P. Tikkanen, *At. Data Nucl. Data Tables* **78**, 1 (2001).
- [61] J. D. Bierman, P. Chan, J. F. Liang, M. P. Kelly, A. A. Sonzogni, and R. Vandenbosch, *Phys. Rev. Lett.* **76**, 1587 (1996).
- [62] H. Zhang, J. Xu, Z. Liu, J. Lu, M. Ruan, and K. Xu, *Phys. Rev. C* **42**, 1086 (1990).
- [63] T. Banerjee, S. Nath, and S. Pal, *Phys. Rev. C* **91**, 034619 (2015).
- [64] A. M. Samant, S. Kailas, A. Chatterjee, A. Shrivastava, A. Navin, and P. Singh, *Eur. Phys. J. A* **7**, 59 (2000).
- [65] Y. X. Watanabe, A. Yoshida, T. Fukuda, T. Sekine, Y. Watanabe, H. Ikezoe, Y. Nagame, T. Ikuta, I. Nishinaka, Y. Mizoi, J. Nakano, M. Hirai, H. Sakurai, H. Kobinata, Y. Pu, K. Kimura, and M. Ishihara, *Eur. Phys. J. A* **10**, 373 (2001).
- [66] K. Nishio, H. Ikezoe, S. Mitsuoka, and J. Lu, *Phys. Rev. C* **62**, 014602 (2000).
- [67] S. Mitsuoka, H. Ikezoe, K. Nishio, and J. Lu, *Phys. Rev. C* **62**, 054603 (2000).
- [68] H. Q. Zhang, C. L. Zhang, C. J. Lin, Z. H. Liu, F. Yang, A. K. Nasirov, G. Mandaglio, M. Manganaro, and G. Giardina, *Phys. Rev. C* **81**, 034611 (2010).
- [69] C. R. Morton, A. C. Berriman, R. D. Butt, M. Dasgupta, A. Godley, D. J. Hinde, and J. O. Newton, *Phys. Rev. C* **62**, 024607 (2000).
- [70] A. Wakhle, K. Hammerton, Z. Kohley, D. J. Morrissey, K. Stiefel, J. Yurkon, J. Walshe, K. J. Cook, M. Dasgupta, D. J. Hinde, D. J. Jeung, E. Prasad, D. C. Rafferty, C. Simenel, E. C. Simpson, K. Vo-Phuoc, J. King, W. Loveland, R. Yanez, *Phys. Rev. C* **97**, 021602(R) (2018).
- [71] R. Bock and Y. T. Chu, M. Dakowski *et al.*, *Nucl. Phys. A* **388**, 334 (1982).
- [72] K. Nishio, H. Ikezoe, I. Nishinaka, S. Mitsuoka, K. Hirose, T. Ohtsuki, Y. Watanabe, Y. Aritomo, and S. Hofmann, *Phys. Rev. C* **82**, 044604 (2010).
- [73] M. G. Itkis, I. M. Itkis, G. N. Knyazheva *et al.*, *Nucl. Phys. A* **834**, 374c (2010).
- [74] W. Q. Shen, J. Albinski, A. Gobbi, S. Gralla, K. D. Hildenbrand, N. Herrmann, J. Kuzminski, W. F. J. Miller, H. Stelzer, J. Tke, B. B. Back, S. Bjornholm, and S. P. Srensen, *Phys. Rev. C* **36**, 115 (1987).
- [75] K. Nishio *et al.*, *Phys. Rev. C* **86**, 034608 (2012).
- [76] V. E. Viola, K. Kwiatkowski, and M. Walker, *Phys. Rev. C* **31**, 1550 (1985).
- [77] M. G. Itkis, A. A. Bogachev, and I. M. Itkis *et al.*, *Nucl. Phys. A* **787**, 150 (2007).
- [78] E. M. Kozulin, G. N. Knyazheva, I. M. Itkis *et al.*, *Phys. Rev. C* **90**, 054608 (2014).
- [79] Ş. Mişicu and H. Esbensen, *Phys. Rev. Lett.* **96**, 112701 (2006).
- [80] C. H. Dasso and G. Pollarolo, *Phys. Rev. C* **68**, 054604 (2003).
- [81] Dao T. Khoa, G. R. Satchler, and W. von Oertzen, *Phys. Rev. C* **56**, 954 (1997).
- [82] K. Hagino, K. Ogata, and A. M. Moro, *Prog. Part. Nucl. Phys.* **125**, 103951 (2022).